Three-Dimensional Quantitative Magnetic Resonance Imaging of Epiphyseal Cartilage Vascularity Using Vessel Image Features

New Insights into Juvenile Osteochondritis Dissecans

Jutta M. Ellermann, MD, PhD, Kai D. Ludwig, PhD, Mikko J. Nissi, PhD, Casey P. Johnson, PhD, John P. Strupp, MSEE, Luning Wang, PhD, Štefan Zbýň, PhD, Ferenc Tóth, DVM, PhD, Elizabeth Arendt, MD, Marc Tompkins, MD, Kevin Shea, MD, and Cathy S. Carlson, DVM, PhD

Investigation performed at the University of Minnesota, Minneapolis, Minnesota

Background: We introduce a quantitative measure of epiphyseal cartilage vascularity and examine vessel networks during human skeletal maturation. Understanding early morphological changes in the distal femoral condyle is expected to provide information on the pathogenesis of developmental diseases such as juvenile osteochondritis dissecans.

Methods: Twenty-two cadaveric knees from donors ranging from 1 month to 10 years of age were included in the study. Images of bone, cartilage, and vascularity were acquired simultaneously with a 3-dimensional gradient-recalled-echo magnetic resonance imaging (MRI) sequence. The secondary ossification center volume and total epiphysis cartilage volume ratio and articular-epiphyseal cartilage complex and epiphyseal cartilage widths were measured. Epiphyseal cartilage vascularity was visualized for 9 data sets with quantitative susceptibility mapping and vessel filtering, resulting in 3-dimensional data to inform vessel network segmentation and to calculate vascular density.

Results: Three distinct, non-anastomosing vascular networks (2 peripheral and 1 central) supply the distal femoral epiphyseal cartilage. The central network begins regression as early as 3 months and is absent by 4 years. From 1 month to 3 years, the ratio of central to peripheral vascular area density decreased from 1.0 to 0.5, and the ratio of central to peripheral vascular skeletal density decreased from 0.9 to 0.6. A narrow, peripheral vascular rim was present at 8 years but had disappeared by 10 years. The secondary ossification center progressively acquires the shape of the articular-epiphyseal cartilage complex by 8 years of age, and the central areas of the medial and lateral femoral condyles are the last to ossify.

Conclusions: Using cadaveric pediatric knees, we provide quantitative, 3-dimensional measures of epiphyseal cartilage vascular regression during skeletal development using vessel image features. Central areas with both early vascular regression and delayed ossification correspond to predilection sites of juvenile osteochondritis dissecans in this limited case series. Our findings highlight specific vascular vulnerabilities that may lead to improved understanding of the pathogenesis and better-informed clinical management decisions in developmental skeletal diseases.

Clinical Relevance: This paradigm shift in understanding of juvenile osteochondritis dissecans etiology and disease progression may critically impact future patient management. Our findings highlight specific vascular vulnerabilities during skeletal maturation in a group of active young patients seen primarily by orthopaedic surgeons and sports medicine professionals.
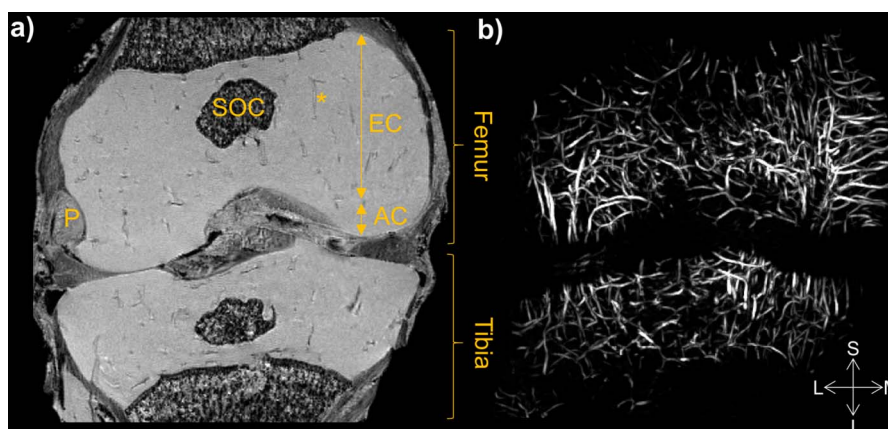
Fig. 1

Figs. 1-A and 1-B Anatomical and vascular MRI scans of a 1-month postnatal knee joint. **Fig. 1-A** A representative magnitude image from the 3-dimensional GRE sequence depicts the femur and tibia of a knee joint in the coronal orientation. Epiphyseal cartilage (EC) and articular cartilage (AC) are of high signal intensity and together encompass the articular-epiphyseal cartilage complex where low-intensity vascular canals (indicated by an asterisk) traverse the EC only. There is a small, low-intensity secondary ossification center (SOC). The popliteus tendon (P) marks the lateral aspect of the knee. **Fig. 1-B** The corresponding quantitative susceptibility mapping post-processed maximum intensity projection demonstrates the vascular network of the EC in both the femur and tibia. S = superior, L = lateral, M = medial, and I = inferior.

There is a growing clinical need to better understand pediatric joint diseases of developmental origin, such as juvenile osteochondritis dissecans[1-3]. These diseases pose a serious burden on affected children, their families, and the health-care system. In the short term, they can negatively impact the self-esteem and social integration of otherwise healthy young patients, and later they can progress to premature osteoarthritis[4]. Unfortunately, research in this area has been scarce, largely because of the lack of appropriate study methods.

Current clinical treatment of juvenile osteochondritis dissecans is hampered by a lack of clear, evidence-based management guidelines[1,2]. Juvenile osteochondritis dissecans is diagnosed in its chronic stage with up to 75% of lesions involving the central aspect of the medial femoral condyle[5-10]. The pathogenesis remains poorly understood[10,11]. A similar disease in animals, osteochondrosis, has
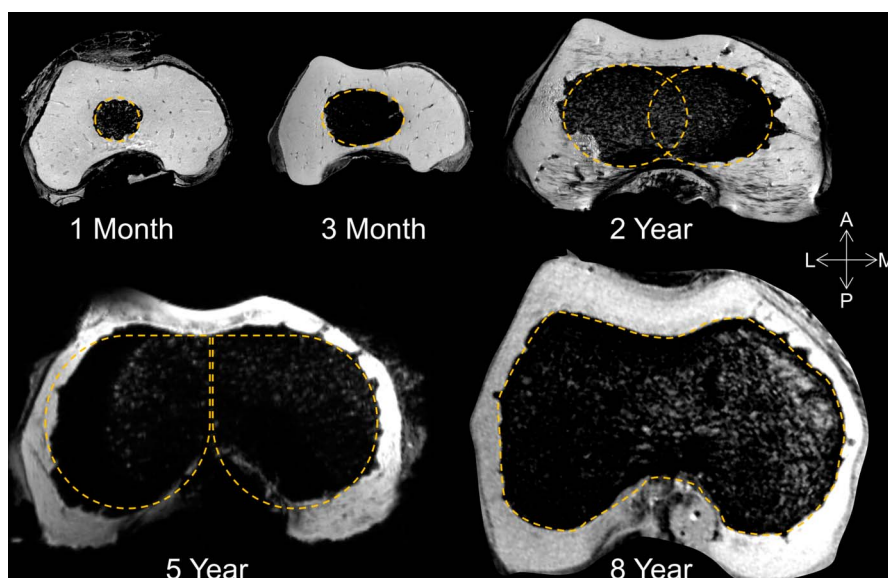
Fig. 2

Secondary ossification center development with age. Representative stages of the development of the secondary ossification center in the axial plane at the level of the maximal trochlear depth. The shape of the secondary ossification center changes from round (1 month), to oval (3 months), to congruent ovals (2 years), to aviator glasses (5 years), to finally assuming the asymmetric (about the midline) contour of the overlying cartilage template of the adult distal femur (8 years). A = anterior, L = lateral, M = medial, and P = posterior.

Fig. 3

The secondary ossification center (SOC) and total epiphysis volume (TEV) change with age. The percentage of volume ratio of the SOC (bone) to TEV (cartilage) increases linearly with age for both sexes.

been demonstrated to be caused by failure of the vascular supply to the epiphyseal cartilage[12-17]; work in cadaveric specimens has strongly suggested that the pathogenesis of the disease in humans is of similar origin[18-20]. Recent clinical magnetic resonance imaging (MRI) studies provided evidence 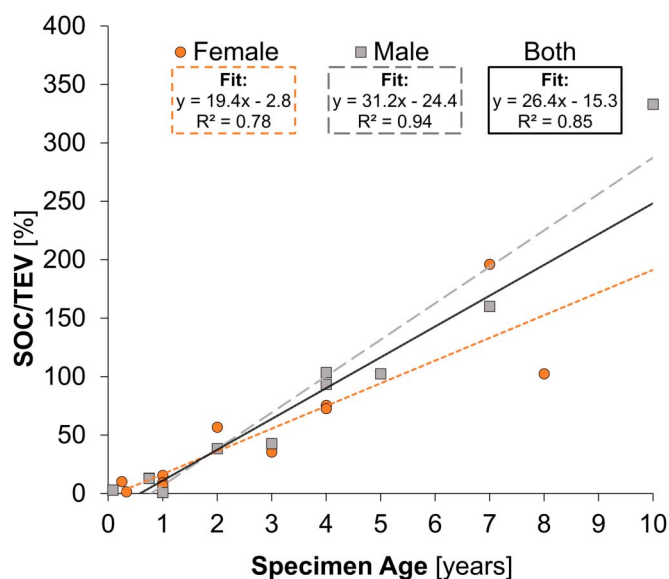on epiphyseal cartilage origin and subsequent osseous manifestation[21] of juvenile osteochondritis dissecans in pediatric patients and described the possible role of the secondary physis in the disease[22].

Although the articular cartilage is avascular, the subarticular epiphyseal cartilage is highly vascular[23-25]. Growth and development during skeletal maturation lead to the gradual replacement of the vascular epiphyseal cartilage with bone via enchondral ossification[26]. Traditionally, the vascular supply could only be studied using invasive techniques[27-29]. Recently, our group described noninvasive MRI approaches, including susceptibility-weighted imaging, to visualize epiphyseal cartilage vascularity[30-32], a method that has been already adapted to animal and human in vivo studies[33,34].

The purpose of this study was to introduce quantitative measures of the entire joint. Utilizing images of bone, cartilage, and vascular canals acquired simultaneously with a single 3-dimensional MRI sequence, we provide a comprehensive visualization of vessel network connectivity, quantification of epiphyseal vascular density, and progressive ossification during normal human skeletal maturation. These measurements constitute a necessary step toward improved clinical assessment tools for orthopaedic developmental diseases of children and young adults.

Materials and Methods

Subjects

Twenty-two cadaveric knee specimens from donors who were 1 month to 10 years of age, provided by AlloSource,

were included in this retrospective case series study. A waiver for institutional review board approval was applied. Eleven of the specimens were from female donors and 11 specimens were from male donors. For each sex, there were 7 unilateral specimens (right or left) and 2 bilateral specimens (same donor,
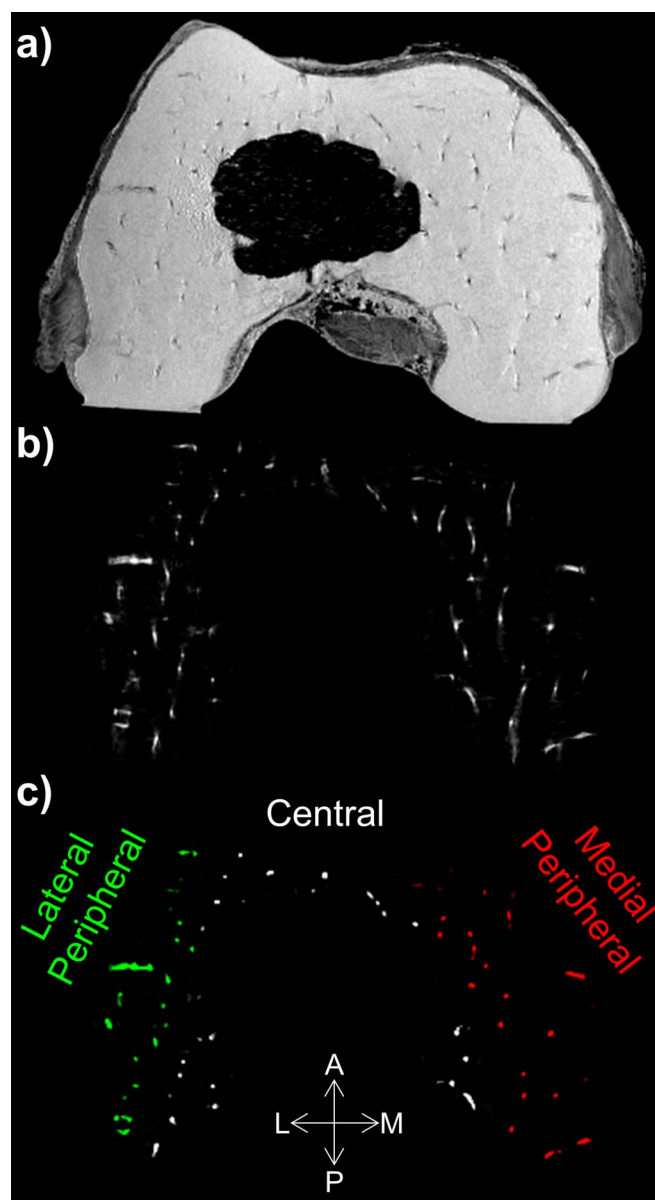
Fig. 4

Figs. 4-A, 4-B, and 4-C Epiphyseal cartilage vascular visualization with MRI. A = anterior, L = lateral, M = medial, and P = posterior. A representative slice of the 3-dimensional GRE MRI data set shows the magnitude anatomical image (**Fig. 4-A**) and vasculature (**Fig. 4-B**) after quantitative susceptibility mapping post-processing. Vessel-enhancement filters and semiautomatic segmentation allows for the vascular supply of the distal femoral epiphyseal cartilage to be visualized as a color-coded vascular network image (**Fig. 4-C**) (lateral peripheral = green vessels, central = white vessels, and medial peripheral = red vessels).

right and left). All knee specimens were presumed to be normal and without evidence of joint disease. Specimens were received frozen at −20°C and were thawed at room temperature immediately prior to MRI. For a description of the intra-epiphyseal vascular supply, we utilized a modification of a previously published nomenclature[27].

MRI

Images of bone, cartilage, and vascularity were acquired simultaneously with a 3-dimensional gradient-recalled-echo (GRE) MRI sequence on specimens between August 2013 and January 2016. The specimens were placed in test tubes immersed in perfluoropolyether to avoid image artifacts introduced by the susceptibility mismatch of tissue-air interfaces. The distal femoral specimens were oriented with the femoral diaphysis along the main magnetic field. Smaller specimens (n = 7) were imaged using a preclinical 9.4-T MRI system (31-cm bore; Agilent Technologies) and a quadrature volume transceiver coil (Millipede; Varian NMR Systems). The GRE sequence used a repetition time (TR)/echo time (TE) = 40/15 ms, flip angle = 15°, matrix = 384 × 384 × 384, resolution = ~100 μm isotropic, and acquisition bandwidth = 43 Hz/voxel. Larger specimens (n = 15) were imaged using a whole-body, 7.0-T MR system (MAGNETOM; Siemens Healthineers) with an 8-channel transmit/receive knee coil (Virtumed) driven by a B_1^+ shimming unit (CPC) with 8 × 1 kW amplifiers. At 7 T, the GRE sequence used a TR/TE = 45/29 ms, flip angle = 25°, matrix = up to 384 × 384 × 176, resolution = ~320 μm isotropic, and acquisition bandwidth = 60 Hz/voxel. Transmit B_1^+ shimming was performed to maximize excitation homogeneity using a fast estimation technique from B_1^+ maps as previously described[30,35].

Data Analysis

Three-dimensional visualization of the vascular structures in the epiphyseal cartilage was achieved using quantitative susceptibility mapping post-processing[30,35]. Briefly, the GRE phase images were preprocessed to remove wrapping artifacts and background field contributions utilizing masks comprising the articular-epiphyseal cartilage complex[36-39]. A regularized quantitative susceptibility mapping method[40] was used to estimate the susceptibility distribution in the articular-epiphyseal cartilage complex using MATLAB (MathWorks)[30], which was then loaded into OsiriX (Pixmeo) for visualization of the intra-epiphyseal vascular supply. A board-certified musculoskeletal radiologist with >10 years of experience performed a qualitative evaluation of changes in the vascular supply of the distal femoral condyle and the morphological growth of the joint.

To pilot our vessel-filtering post-processing algorithm for 3-dimensional MRI data[41], the vascular network of the epiphyseal cartilage was analyzed in a subset of 9 specimens, void of obvious degradation, at ages representing developmental milestones. A Hessian-based Frangi filter[42] converted quantitative susceptibility mapping images to vessel-likelihood maps that were subsequently converted to binary vessel masks using a thresholding operation. The binary vessel masks were skeletonized using parallel medial axis thinning[43], and a network graph was calcu-
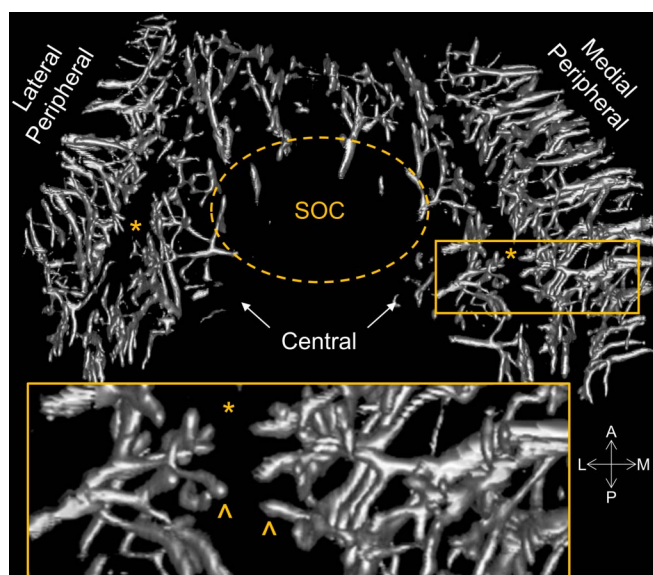

Fig. 5

Distal femoral epiphysis vascular canals at 3-month postnatal development. A volume rendering demonstrates the 2 distinct segmental distributions of the vascular canals with an intervening avascular zone (indicated by the asterisks) surrounding the small secondary ossification center (SOC). The peripheral vascular network consists of the lateral and medial vascular canals, and the central vascular network (arrows) consists of the intercondylar vessels. The inset of a higher-magnification image shows a group of regularly spaced vessels that extend from the periphery to the avascular zone (indicated by the asterisk) in a cluster of terminating small sinusoidal buds (carets). The avascular zone is interposed between the peripheral and central vascular networks; no anastomoses are observed between these 2 sources of blood supply. A = anterior, L = lateral, M = medial, and P = posterior.

lated[44]. The 2 peripheral and single central vascular networks were segmented by manually selecting initial boundary seed points on the network graph for each region. Then an automatic region-growing algorithm enclosed the selected seeds and grew outwardly to the edges of the articular-epiphyseal cartilage complex mask, defining each vascular region simultaneously. The vascular area density was calculated using the binary vessel mask, and the vascular skeletal density (density measure independent of vessel thickness) was calculated using the skeletonized vessel mask[45]. The vascular area density and vascular skeletal density for the peripheral network, both medial and lateral sides combined, were normalized to the central network to account for post-processing variations across specimens.

The secondary ossification center and articular-epiphyseal cartilage complex of the distal femoral epiphysis were manually segmented using OsiriX from 3-dimensional GRE images, and the ratio of the secondary ossification center volume to the total epiphysis volume, defined as the secondary ossification center volume plus the articular-epiphyseal cartilage complex volume, was calculated. The articular-epiphyseal cartilage complex and epiphyseal cartilage widths on the lateral and medial condyle were measured in the axial orientation for all specimens.
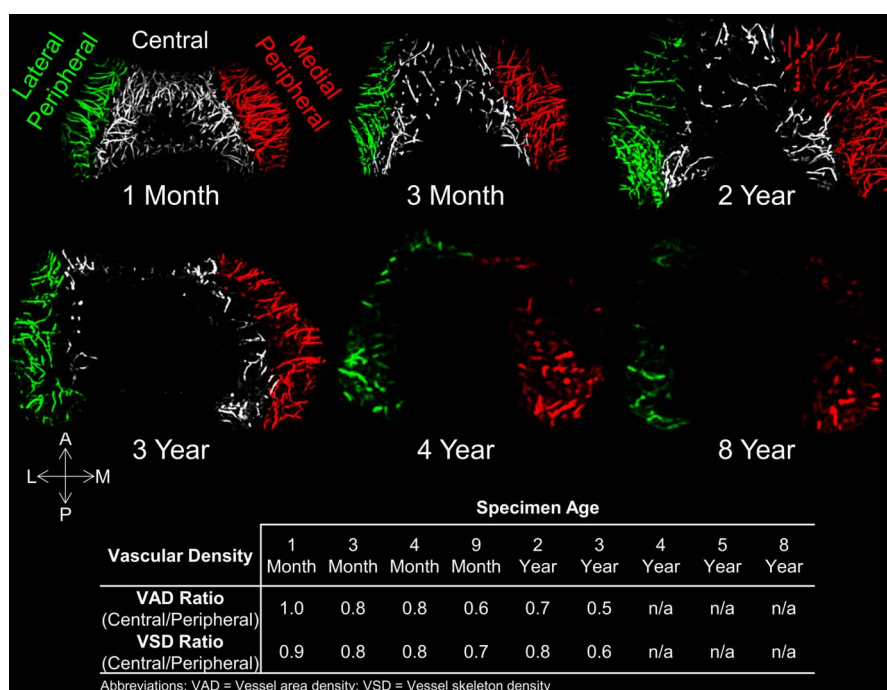
Fig. 6

Visualizations and density changes in vascular network with age. Maximum-intensity projections of the quantitative susceptibility mapping-post-processed, vessel-enhanced maps from 6 selected cadaveric specimens with increasing age are shown in the top 2 rows. The vasculature is color-coded according to the vascular network (lateral peripheral = green vessels, central = white, and medial peripheral = red). The embedded table summarizes the density ratio measurements (vascular area density and vascular skeletal density) of the central network to the peripheral (medial and lateral) network. No central network was observed in the specimens from donors who were ≥4 years of age. By 8 years of age, there was a small, residual peripheral vascular network. At 10 years of age, no epiphyseal cartilage vascularity could be detected. A = anterior, L = lateral, M = medial, P = posterior, and n/a = not available.

Statistics

A paired Student t test was performed between the medial and lateral epiphyseal cartilage widths, both of which were normalized to the articular-epiphyseal cartilage complex width, with significance set at $p < 0.05$.

Results

Advanced processing of 3-dimensional GRE images offers a high-resolution visualization of the vascular network within the epiphyseal cartilage of the knee. A representative GRE magnitude image from a cadaveric specimen from a 1-month-old donor is shown in Figure 1-A and demonstrates the anatomical locations of the articular cartilage, epiphyseal cartilage, and secondary ossification center within the femur of the right knee joint. The corresponding maximum intensity projection of quantitative susceptibility mapping images in Figure 1-B showed the vascular canals contained within both the femoral epiphyseal cartilage and the tibial epiphyseal cartilage, and no canals were observed in the articular cartilage.

The secondary ossification center volume increased and changed shape throughout development (Fig. 2). The contour of the secondary ossification center progressed from round (1 month), to oval (3 months), to congruent ovals (2 years), to the shape of aviator glasses (5 years). Between the ages of 2 and 5 years, the transverse (medial-lateral) dimension of the sec-

ondary ossification center appeared greater in width than its anterior-posterior dimension. The secondary ossification center changes were symmetric about the midline from 1 month up
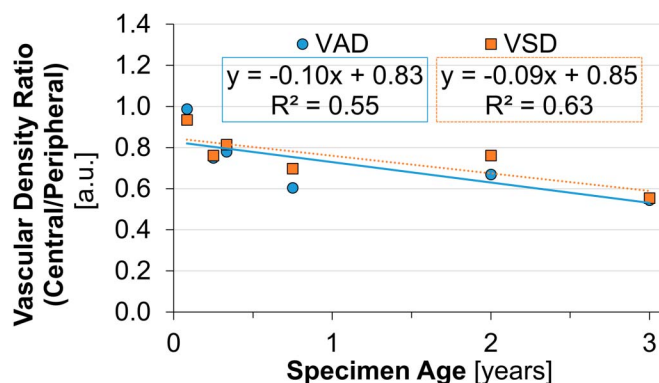
Fig. 7

Vascular density compared with specimen age. Quantitative vascular density measurements (displayed as a ratio of the central vascular network to the peripheral vascular network) for the selected 6 specimens containing a central vascular network (<3 years of age). A linear fit showed a decreasing trend in the central and peripheral vascular area density (VAD) and vascular skeletal density (VSD) ratios with specimen age up to 3 years. a.u. = arbitrary units.
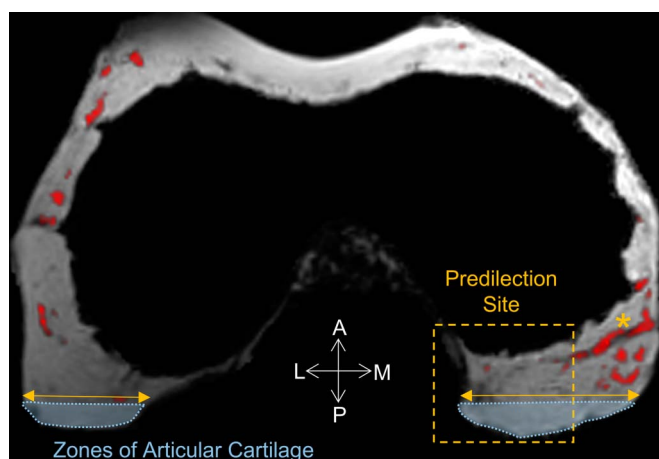
Fig. 8

MRI visualization of the vascular supply to the predilection site. A representative axial slice of the distal part of the femur from the 3-dimensional GRE MRI data set from a 5-year-old specimen shows the magnitude image (gray scale) overlaid with the vascular post-processed image (red scale). The central vascular supply has vanished. The ossification front has reached the central aspect of the intercondylar notch and grew wider in the transverse than the anteroposterior dimension leaving the thickest not-yet-ossified cartilage at the weight-bearing aspect of the joint. The articular cartilage (denoted by a light blue dotted line) is free of vessels; therefore, the subarticular epiphyseal cartilage vascular supply has to travel from the peripheral extra-articular perichondrium in parallel to the articular surface to reach the central aspect of the medial and lateral femoral condyles. This leaves these areas at the central aspect of the medial femoral condyle (wider), and to a lesser degree the lateral femoral condyle, most distant to the origin of their peripheral vascular supply. The predilection site of juvenile osteochondritis dissecans (highlighted) and a medial-lateral running vascular canal from the peripheral vascular supply is marked (denoted by an asterisk). A = anterior, L = lateral, M = medial, and P = posterior.

until approximately 5 years of age. During the early development, the secondary ossification center did not resemble the shape of the articular-epiphyseal cartilage complex template, and, by approximately 7 to 8 years of age, the secondary ossification center acquired the asymmetric shape of the articular-epiphyseal cartilage complex.

In contrast, the articular-epiphyseal cartilage complex assumed the adult shape at all stages of development, effectively providing a preformed cartilaginous template of the distal part of the femur as early as 1 month (Fig. 2). The articular-epiphyseal cartilage complex gradually increased in size with age (Appendix Fig. S1a) while qualitatively maintaining the asymmetric (lateral compared with medial) shape of the cartilaginous template of the condyles from 1 month to 10 years of age. The secondary ossification center in the center of the distal femoral epiphysis in the 1-month-old specimen occupied <3% of the epiphysis volume. Approximately 50% of the epiphysis volume was occupied by the secondary ossification center at 5 years of age. The ratio of the secondary ossification center to the total epiphysis volume increased approximately linearly

with age for both sexes (Fig. 3). The enchondral ossification in the epiphyseal cartilage appeared to occur at a faster pace in the male specimens than in the female specimens in our sample group. These ratios for the left and right distal femoral condyles of an individual subject were similar, as expected. The secondary ossification center volume and total epiphysis volume were measured for all specimens between the ages of 1 month and 10 years (Appendix Table S1).

A color-coded visualization of the epiphyseal cartilage vascular canals shows a highly ordered vascular network based on a segmental distribution (Fig. 4). A volume rendering for a 3-month-old specimen depicts the epiphyseal vascular canals penetrating the epiphyseal cartilage from the perichondrium and intercondylar notch in a radiating fashion, supplying the epiphyseal cartilage with a peripheral network, which consists of the lateral and medial vascular canals, and the central vascular network, which consists of the intercondylar vessels (Fig. 5). The vascular networks lack connecting anastomoses, leaving a narrow, linear watershed zone of avascular cartilage between vascular networks in both medial and lateral condyles. Each vascular canal terminated in a small sinusoidal bud that was visualized in detail using the 3-dimensional quantitative susceptibility mapping data (Fig. 5, inset).

The central network begins regression as early as 3 months and is absent by 4 years. Although the number of intra-epiphyseal vascular canals decreased with increasing age in all vascular networks, the relative decrease in number of vessels varied by location. Specifically, by 1 to 2 years of age, there was a substantial loss of central vessels in the intercondylar area of both the medial and lateral femoral condyles, as evidenced by a paucity of central epiphyseal vascular canals. The ratio of central to peripheral vascular area density decreased (from 1.0 to 0.5) and the central and peripheral vascular skeletal density ratio decreased (from 0.9 to 0.6) from 1 month to 3 years, showing a similar decreasing trend of vessel density across the analyzed specimens (Fig. 6). With the progression of the ossification front toward the intercondylar notch, the central vascular network had already markedly regressed by 3 years (Fig. 6) and was completely absent at approximately 4 years of age. A linear decrease in the central and peripheral vascular density ratios (vascular area density and vascular skeletal density ratios) was observed with increasing age (Fig. 7). The peripheral vascular network continued to regress with increasing age. The residual peripheral vascular network that was identified at 8 years of age had largely vanished at 10 years of age. The superficial weight-bearing articular cartilage was avascular at all observed time points (age, 1 month to 10 years).

During morphogenesis, the secondary ossification center first was observed at the central aspects of both femoral condyles, as expected. Subsequently, the secondary ossification center predominantly grew to reach the extra-articular peripheral perichondrium. The weight-bearing aspects of both femoral condyles are last to be reached by the secondary ossification center as seen in the 5-year-old distal femoral specimen in Figure 8. The weight-bearing surface is covered with avascular articular

cartilage. The transverse epiphyseal cartilage width normalized to the articular-epiphyseal cartilage complex width was significantly greater (p < 0.001) in the medial compared with the lateral femoral condyle (Appendix Table S1), with a mean difference (and standard deviation) of 11% ± 6%. Epiphyseal cartilage width also increased with specimen age (Appendix Fig. S1b). This leaves areas at the central aspect of the wider medial femoral condyle and, to a lesser degree, the lateral femoral condyle most distant from the origin of their peripheral vascular supply.

Discussion

The most substantial finding from this study was that both early vascular regression and late enchondral ossification during skeletal maturation were demonstrated in areas that coincide with known predilection sites of juvenile osteochondritis dissecans. Our results demonstrate that the specific vascular architecture leaves the wider, last-to-ossify medial femoral condyle, where up to 75% of juvenile osteochondritis dissecans lesions occur[5-9], most distant from the residual peripheral vascular supply.

Importantly, our observations on age-dependent milestones of vascular regression and juvenile osteochondritis dissecans were supported by a recent, very large retrospective demographic study with >1 million patients in this cohort[10]. No juvenile osteochondritis dissecans lesions of the knee were found in children who were 2 to 5 years of age, supporting the notion that the presence of both central and peripheral vascular beds up until 4 years of age as identified in our study might protect from clinically apparent lesions. The earliest manifestation at 6 years reported in this cohort coincides with our findings on regression of the peripheral vascularity between 4 and 10 years of age after the central vascular bed had already largely regressed at 4 years of age. The incidence of juvenile osteochondritis dissecans in individuals who were 6 to 19 years of age was low overall and was reported to be 9.5 per 100,000, with 6.8 cases per 100,000 for those who were between 6 and 11 years of age compared with 11.2 cases per 100,000 for those who were between 12 and 19 years of age[10]. It seems plausible that early lesions may present in the presence of residual peripheral vascularity between the ages of 6 and 11 years, but it takes progression to later stages between the ages of 12 and 19 years for them to become clinically symptomatic at a slightly higher rate. These findings are also consistent with a recent clinical MRI study[21] that found an age-dependence depiction of epiphyseal cartilage lesion progression.

Shared architecture of vascularity and proposed similar pathogenesis of juvenile osteochondritis dissecans between pigs and humans were previously reported by our group[18] based on 5 human specimens and 3 pig specimens. The current study provides a much larger sample size that enabled, for the first time, quantitative measures of the relative vascular density within the epiphyseal cartilage using a vessel-filtering algorithm, which has not previously been done. The new quantitative data add important new knowledge that is particularly relevant for accuracy in future patient studies. When putting our findings into the context of large population cohorts, there is overwhelming evidence that, although pigs have a rampant prevalence of the disease[46], juvenile osteochondritis dissecans is rare in children and adolescents, despite evidence of shared vulnerabilities. That allows for promising conclusions that lesions might be clinically unimportant in humans, unless cofounding independent risk factors[6] come into play.

Overuse in active children is an independent risk factor for developmental diseases such as juvenile osteochondritis dissecans[22,47-49]. Approximately 60% to 75% of weight-bearing forces through the knee are normally transmitted through the medial compartment[50-53]. An association between the biomechanical loading including overweight and juvenile osteochondritis dissecans location exists[9,54,55]. This implies that, once risk factors have been identified, preventive measures could be implemented. Furthermore, understanding the pathophysiology of juvenile osteochondritis dissecans as a delay in enchondral ossification due to the failure of vascular transfer from epiphyseal cartilage to the secondary ossification center with associated chondronecrosis in children[21] would warrant new treatment approaches. A shift toward early detection and management is taking place in our clinical practice at the University of Minnesota, a referral center for juvenile osteochondritis dissecans; 2 to 3 years ago, the majority of patients referred for MRI were 13 to 20 years of age, and mostly osseous lesions were detected. Now, patients are younger, between 5 and 12 years of age, and increasingly cartilaginous lesions are identified (Tompkins M, University of Minnesota. Personal communication; 2019 Jun 4). Routinely, we utilize the clinical sequence described in this article to differentiate between cartilaginous and osseous lesions, information that is currently unattainable with clinical turbo-spin-echo sequences[21]. Epiphyseal cartilage vascular imaging in children has been shown to be feasible clinically at 3 T[56] and at 7 T[34]; recently, the U.S. Food and Drug Administration (FDA) approved epiphyseal cartilage vascular imaging for clinical use in patients who weighed >30 kg. Alterations in epiphyseal cartilage vascularity are important in other diseases, such as infection, juvenile arthritis[57], Legg-Calvé-Perthes disease[58], Osgood-Schlatter disease, mucopolysaccharidosis[59], and failure of osteogenesis[60] during skeletal development.

This study had several major limitations. First, the number of specimens and the age and sex distribution depended on their availability. Unfortunately, these specimens were few in number and the ages and sex distribution were unpredictable. This limitation precluded a prospective study based on power calculations. Furthermore, the small sample size limited a statistical comparison between male and female specimens to identify sex differences. Vascular variations within an age range or between left and right knees were not evaluated because we had limited specimen numbers and this would require larger, population-based studies. Second, the conclusions drawn in this report were based on high-resolution ex vivo results. Additional in vivo studies are warranted to prove technical translatability and clinical utility. The clinical impact will need to be determined in future studies. Lastly, our data did not prove a direct cause-and-effect relationship between vascular regression and occurrence of juvenile osteochondritis

dissecans. Instead, the data provided evidence of complex, multifactorial relationships between local age-dependent vulnerabilities at predilection sites of juvenile osteochondritis dissecans, biomechanical loading, shear forces, and unknown genetic predisposition. Future studies are needed to shed more light into these complex interactions.

In conclusion, this study provides simultaneously acquired, quantitative, 3-dimensional MRI measures of the regressing epiphyseal cartilage vascularity during skeletal development using vessel image features, as well as bone and cartilage volumes. In pursuit of a paradigm shift toward precision medicine, the introduced quantitative approach can serve as a tool for necessary further clinical studies.

Appendix

(eA) Supporting material provided by the authors is posted with the online version of this article as a data supplement at jbjs.org (http://links.lww.com/JBJSOA/A131). ∎

Jutta M. Ellermann, MD, PhD[1]
Kai D. Ludwig, PhD[1]
Mikko J. Nissi, PhD[1,2]
Casey P. Johnson, PhD[1,3]
John P. Strupp, MSEE[1]
Luning Wang, PhD[1]
Štefan Zbýň, PhD[1]
Ferenc Tóth, DVM, PhD[3]

Elizabeth Arendt, MD[1]
Marc Tompkins, MD[1]
Kevin Shea, MD[4]
Cathy S. Carlson, DVM, PhD[3]

[1]Center for Magnetic Resonance Research (CMRR) (J.M.E., K.D.L., M.J.N., C.P.J., J.P.S., L.W., and S.Z.), Department of Radiology, and Department of Orthopaedic Surgery (E.A. and M.T.), Medical School, University of Minnesota, Minneapolis, Minnesota

[2]Department of Applied Physics, University of Eastern Finland, Kuopio, Finland

[3]Departments of Veterinary Population Medicine (F.T.) and Veterinary Clinical Sciences (C.P.J.,C.S.C.), College of Veterinary Medicine, University of Minnesota, St. Paul, Minnesota

[4]Department of Orthopaedic Surgery, Stanford University, Stanford, California

Email address for J.M. Ellermann: eller001@umn.edu

ORCID iD for J.M. Ellermann: 0000-0002-7109-9656
ORCID iD for K.D. Ludwig: 0000-0001-9867-9346
ORCID iD for M.J. Nissi: 0000-0002-5678-0689
ORCID iD for C.P. Johnson: 0000-0001-9826-7296
ORCID iD for J.P. Strupp: 0000-0002-1728-3380
ORCID iD for L. Wang: 0000-0003-0799-4469
ORCID iD for Š. Zbýň: 0000-0002-8211-2828
ORCID iD for F. Tóth: 0000-0002-6615-389X
ORCID iD for E. Arendt: 0000-0002-6944-7332
ORCID iD for M. Tompkins: 0000-0002-8641-3150
ORCID iD for K. Shea: 0000-0002-4160-0163
ORCID iD for C.S. Carlson: 0000-0002-0355-5525

References

1. Chambers HG, Shea KG, Anderson AF, Jojo Brunelle TJ, Carey JL, Ganley TJ, Paterno M, Weiss JM, Sanders JO, Watters WC 3rd, Goldberg MJ, Keith MW, Turkelson CM, Wies JL, Raymond L, Boyer KM, Hitchcock K, Sluka P, Boone C, Patel N; American Academy of Orthopaedic Surgeons. American Academy of Orthopaedic Surgeons clinical practice guideline on: the diagnosis and treatment of osteochondritis dissecans. J Bone Joint Surg Am. 2012 Jul 18;94(14):1322-4.

2. Chambers HG, Shea KG, Carey JL. AAOS Clinical Practice Guideline: diagnosis and treatment of osteochondritis dissecans. J Am Acad Orthop Surg. 2011 May;19(5):307-9.

3. Cruz AI Jr, Shea KG, Ganley TJ. Pediatric knee osteochondritis dissecans lesions. Orthop Clin North Am. 2016 Oct;47(4):763-75. Epub 2016 Aug 6.

4. Edmonds EW, Shea KG. Osteochondritis dissecans: editorial comment. Clin Orthop Relat Res. 2013 Apr;471(4):1105-6.

5. Cooper T, Boyles A, Samora WP, Klingele KE. Prevalence of bilateral JOCD of the knee and associated risk factors. J Pediatr Orthop. 2015 Jul-Aug;35(5):507-10.

6. Edmonds EW, Polousky J. A review of knowledge in osteochondritis dissecans: 123 years of minimal evolution from König to the ROCK study group. Clin Orthop Relat Res. 2013 Apr;471(4):1118-26.

7. Lindén B. The incidence of osteochondritis dissecans in the condyles of the femur. Acta Orthop Scand. 1976 Dec;47(6):664-7.

8. Ellermann JM, Donald B, Rohr S, Takahashi T, Tompkins M, Nelson B, Crawford A, Rud C, Macalena J. Magnetic resonance imaging of osteochondritis dissecans: validation study for the ICRS classification system. Acad Radiol. 2016 Jun;23(6):724-9. Epub 2016 Mar 11.

9. Gonzalez-Herranz P, Rodriguez ML, de la Fuente C. Femoral osteochondritis of the knee: prognostic value of the mechanical axis. J Child Orthop. 2017;11(1):1-5.

10. Kessler JI, Nikizad H, Shea KG, Jacobs JC Jr, Bebchuk JD, Weiss JM. The demographics and epidemiology of osteochondritis dissecans of the knee in children and adolescents. Am J Sports Med. 2014 Feb;42(2):320-6. Epub 2013 Nov 22.

11. Bruns J, Werner M, Habermann C. Osteochondritis dissecans: etiology, pathology, and imaging with a special focus on the knee joint. Cartilage. 2018 Oct;9(4):346-62. Epub 2017 Jun 22.

12. Olsson SE, Reiland S. The nature of osteochondrosis in animals. Summary and conclusions with comparative aspects on osteochondritis dissecans in man. Acta Radiol Suppl. 1978;358:299-306.

13. Carlson CS, Hilley HD, Henrikson CK, Meuten DJ. The ultrastructure of osteochondrosis of the articular-epiphyseal cartilage complex in growing swine. Calcif Tissue Int. 1986 Jan;38(1):44-51.

14. Carlson CS, Meuten DJ, Richardson DC. Ischemic necrosis of cartilage in spontaneous and experimental lesions of osteochondrosis. J Orthop Res. 1991 May;9(3):317-29.

15. Ytrehus B, Ekman S, Carlson CS, Teige J, Reinholt FP. Focal changes in blood supply during normal epiphyseal growth are central in the pathogenesis of osteochondrosis in pigs. Bone. 2004 Dec;35(6):1294-306.

16. Olstad K, Ytrehus B, Ekman S, Carlson CS, Dolvik NI. Epiphyseal cartilage canal blood supply to the distal femur of foals. Equine Vet J. 2008 Jul;40(5):433-9.

17. Olstad K, Ekman S, Carlson CS. An update on the pathogenesis of osteochondrosis. Vet Pathol. 2015 Sep;52(5):785-802. Epub 2015 Jun 16.

18. Tóth F, Nissi MJ, Ellermann JM, Wang L, Shea KG, Polousky J, Carlson CS. Novel application of magnetic resonance imaging demonstrates characteristic differences in vasculature at predilection sites of osteochondritis dissecans. Am J Sports Med. 2015 Oct;43(10):2522-7. Epub 2015 Aug 18.

19. Tóth F, Tompkins MA, Shea KG, Ellermann JM, Carlson CS. Identification of areas of epiphyseal cartilage necrosis at predilection sites of juvenile osteochondritis dissecans in pediatric cadavers. J Bone Joint Surg Am. 2018 Dec 19;100(24):2132-9.

20. McCoy AM, Toth F, Dolvik NI, Ekman S, Ellermann J, Olstad K, Ytrehus B, Carlson CS. Articular osteochondrosis: a comparison of naturally-occurring human and animal disease. Osteoarthritis Cartilage. 2013 Nov;21(11):1638-47. Epub 2013 Aug 15.

21. Ellermann J, Johnson CP, Wang L, Macalena JA, Nelson BJ, LaPrade RF. Insights into the epiphyseal cartilage origin and subsequent osseous manifestation of juvenile osteochondritis dissecans with a modified clinical MR imaging protocol: a pilot study. Radiology. 2017 Mar;282(3):798-806. Epub 2016 Sep 15.

22. Laor T, Zbojniewicz AM, Eismann EA, Wall EJ. Juvenile osteochondritis dissecans: is it a growth disturbance of the secondary physis of the epiphysis? AJR Am J Roentgenol. 2012 Nov;199(5):1121-8.

23. Lutfi AM. Mode of growth, fate and functions of cartilage canals. J Anat. 1970 Jan;106(Pt 1):135-45.

24. Wilsman NJ, Van Sickle DC. Cartilage canals, their morphology and distribution. Anat Rec. 1972 May;173(1):79-93.

25. Blumer MJ, Longato S, Fritsch H. Structure, formation and role of cartilage canals in the developing bone. Ann Anat. 2008;190(4):305-15. Epub 2008 May 28.

26. Camacho-Hübner C, Nilsson O, Sävendahl L. Cartilage and bone development and its disorders. Karger; 2011.

27. Crock HV. The arterial supply and venous drainage of the bones of the human knee joint. Anat Rec. 1962 Nov;144:199-217.

28. Scapinelli R. Studies on the vasculature of the human knee joint. Acta Anat (Basel). 1968;70(3):305-31.

29. Shapiro F. Epiphyseal and physeal cartilage vascularization: a light microscopic and tritiated thymidine autoradiographic study of cartilage canals in newborn and young postnatal rabbit bone. Anat Rec. 1998 Sep;252(1):140-8.

30. Nissi MJ, Tóth F, Wang L, Carlson CS, Ellermann JM. Improved visualization of cartilage canals using quantitative susceptibility mapping. PLoS One. 2015 Jul 13; 10(7):e0132167.

31. Nissi MJ, Toth F, Zhang J, Schmitter S, Benson M, Carlson CS, Ellermann JM. Susceptibility weighted imaging of cartilage canals in porcine epiphyseal growth cartilage ex vivo and in vivo. Magn Reson Med. 2014 Jun;71(6):2197-205. Epub 2013 Jul 15.

32. Tóth F, Nissi MJ, Zhang J, Benson M, Schmitter S, Ellermann JM, Carlson CS. Histological confirmation and biological significance of cartilage canals demonstrated using high field MRI in swine at predilection sites of osteochondrosis. J Orthop Res. 2013 Dec;31(12):2006-12. Epub 2013 Aug 12.

33. Kolb A, Robinson S, Stelzeneder D, Schreiner M, Chiari C, Windhager R, Trattnig S, Bohndorf K. Vessel architecture in human knee cartilage in children: an in vivo susceptibility-weighted imaging study at 7 T. Eur Radiol. 2018 Aug;28(8):3384-92. Epub 2018 Feb 26.

34. Dymerska B, Bohndorf K, Schennach P, Rauscher A, Trattnig S, Robinson SD. In vivo phase imaging of human epiphyseal cartilage at 7 T. Magn Reson Med. 2018 Apr;79(4):2149-55. Epub 2017 Jul 31.

35. Nissi MJ, Tóth F, Carlson C, Shea K, Polousky J, Ellermann J. MRI visualization of cartilage canal vessels in cadaveric human epiphyseal growth cartilage. Presented as a poster exhibit at the ORS (Orthopaedic Research Society) 2014 Annual Meeting; 2014 Mar 15-18; New Orleans, LA. Poster no. 0233.

36. Reichenbach JR, Venkatesan R, Schillinger DJ, Kido DK, Haacke EM. Small vessels in the human brain: MR venography with deoxyhemoglobin as an intrinsic contrast agent. Radiology. 1997 Jul;204(1):272-7.

37. Haacke EM, Xu Y, Cheng YC, Reichenbach JR. Susceptibility weighted imaging (SWI). Magn Reson Med. 2004 Sep;52(3):612-8.

38. Schweser F, Deistung A, Lehr BW, Reichenbach JR. Quantitative imaging of intrinsic magnetic tissue properties using MRI signal phase: an approach to in vivo brain iron metabolism? Neuroimage. 2011 Feb 14;54(4):2789-807. Epub 2010 Oct 30.

39. Bilgic B, Fan AP, Polimeni JR, Cauley SF, Bianciardi M, Adalsteinsson E, Wald LL, Setsompop K. Fast quantitative susceptibility mapping with L1-regularization and automatic parameter selection. Magn Reson Med. 2014 Nov;72(5):1444-59. Epub 2013 Nov 20.

40. Shmueli K, de Zwart JA, van Gelderen P, Li TQ, Dodd SJ, Duyn JH. Magnetic susceptibility mapping of brain tissue in vivo using MRI phase data. Magn Reson Med. 2009 Dec;62(6):1510-22.

41. Ludwig K, Strupp J, Johnson C, Zbyn S, Nissi M, Tóth F, Shea K, Carlson C, Ellermann J. Visualization and quantification of epiphyseal cartilage vasculature using quantitative susceptibility maps of pediatric knee specimens. Presented as a poster exhibit at the ISMRM (International Society of Magnetic Resonance in Medicine) 27th Annual Meeting & Exhibition; 2019 May 11-16; Montreal, Canada. Poster no. 168.

42. Frangi AF, Niessen WJ, Viergever MA. Multiscale vessel enhancement filtering. In: Proceedings of the First International Conference on Medical Image Computing and Computer-Assisted Intervention. 1998 Oct 11-13. Cambridge, MA. Springer; 1998. p. 130-7.

43. Kerschnitzki M, Kollmannsberger P, Burghammer M, Duda GN, Weinkamer R, Wagermaier W, Fratzl P. Architecture of the osteocyte network correlates with bone material quality. J Bone Miner Res. 2013 Aug;28(8):1837-45.

44. Lee TC, Kashyap RL, Chu CN. Building skeleton models via 3-D medial surface axis thinning algorithms. CVGIP Graph Models Image Process. 1994;56(6):462-78.

45. Chu Z, Lin J, Gao C, Xin C, Zhang Q, Chen CL, Roisman L, Gregori G, Rosenfeld PJ, Wang RK. Quantitative assessment of the retinal microvasculature using optical coherence tomography angiography. J Biomed Opt. 2016 Jun 1;21(6):66008.

46. Ytrehus B, Grindflek E, Teige J, Stubsjøen E, Grøndalen T, Carlson CS, Ekman S. The effect of parentage on the prevalence, severity and location of osteochondrosis in swine. J Vet Med A Physiol Pathol Clin Med. 2004 May;51(4):188-95.

47. Wall E, Von Stein D. Juvenile osteochondritis dissecans. Orthop Clin North Am. 2003 Jul;34(3):341-53.

48. Polousky JD. Juvenile osteochondritis dissecans. Sports Med Arthrosc Rev. 2011 Mar;19(1):56-63.

49. Patel DR, Villalobos A. Evaluation and management of knee pain in young athletes: overuse injuries of the knee. Transl Pediatr. 2017 Jul;6(3):190-8.

50. Morrison JB. The mechanics of the knee joint in relation to normal walking. J Biomech. 1970 Jan;3(1):51-61.

51. Andriacchi TP. Dynamics of knee malalignment. Orthop Clin North Am. 1994 Jul; 25(3):395-403.

52. Hsu RW, Himeno S, Coventry MB, Chao EY. Normal axial alignment of the lower extremity and load-bearing distribution at the knee. Clin Orthop Relat Res. 1990 Jun; 255:215-27.

53. Sherman SL, Thompson SF, Clohisy JCF. Distal femoral varus osteotomy for the management of valgus deformity of the knee. J Am Acad Orthop Surg. 2018 May 1; 26(9):313-24.

54. Jacobi M, Wahl P, Bouaicha S, Jakob RP, Gautier E. Association between mechanical axis of the leg and osteochondritis dissecans of the knee: radiographic study on 103 knees. Am J Sports Med. 2010 Jul;38(7):1425-8. Epub 2010 Mar 29.

55. Kessler J, Koebnick C, Smith N, Adams A. Childhood obesity is associated with increased risk of most lower extremity fractures. Clin Orthop Relat Res. 2013 Apr; 471(4):1199-207.

56. Ellermann J, Wang L, Toth F, Shea K, Carlson C, Nissi MJ. New insights into the predilection sites of juvenile osteochondritis dissecans using quantitative susceptibility mapping. Presented as a poster exhibit at the ISMRM (International Society of Magnetic Resonance in Medicine) 25th Annual Meeting & Exhibition; 2017 Apr 22-27; Honolulu, HI. Poster no. 656.

57. Jaimes C, Chauvin NA, Delgado J, Jaramillo D. MR imaging of normal epiphyseal development and common epiphyseal disorders. Radiographics. 2014 Mar-Apr; 34(2):449-71.

58. Johnson CP, Wang L, Tóth F, Aruwajoye O, Kirkham B, Carlson CS, Kim HKW, Ellermann JM. Quantitative susceptibility mapping detects neovascularization of the epiphyseal cartilage after ischemic injury in a piglet model of Legg-Calvé-Perthes disease. J Magn Reson Imaging. 2019 Jul;50(1):106-13. Epub 2018 Dec 17.

59. Zustin J. Morquio disease: the role of cartilage canals in the pathogenesis of chondrogenic dwarfism. Med Hypotheses. 2010 Dec;75(6):642-4. Epub 2010 Aug 25.

60. Holmbeck K, Bianco P, Caterina J, Yamada S, Kromer M, Kuznetsov SA, Mankani M, Robey PG, Poole AR, Pidoux I, Ward JM, Birkedal-Hansen H. MT1-MMP-deficient mice develop dwarfism, osteopenia, arthritis, and connective tissue disease due to inadequate collagen turnover. Cell. 1999 Oct 1;99(1):81-92.